ARTICLES
https://doi.org/10.1038/s41566-019-0503-6
nature photonics

Wavefront shaping in complex media with a 350 kHz modulator via a 1D-to-2D transform

Omer Tzang[1,3*], Eyal Niv[1,3], Sakshi Singh[1], Simon Labouesse[1], Greg Myatt[2] and Rafael Piestun[1]

Controlling the propagation and interaction of light in complex media has sparked major interest in the past few years. Unfortunately, spatial light modulation devices suffer from limited speed, which precludes real-time applications such as imaging in live tissue. To address this critical problem, we introduce a phase-control technique to characterize complex media based on the use of fast one-dimensional (1D) spatial light modulators and a 1D-to-2D transformation performed by the same medium being analysed. We implement the concept using a microelectromechanical grating light valve with 1,088 degrees of freedom, modulated at 350 kHz, enabling unprecedented high-speed wavefront measurements. We continuously measure the transmission matrix, calculate the optimal wavefront and project a focus through various dynamic scattering samples in real time, all within 2.4 ms per cycle. These results improve the previously achieved wavefront shaping modulation speed by more than an order of magnitude and open new opportunities for optical processing using 1D-to-2D transformations.

Recent developments in the field of wavefront shaping (WFS) have demonstrated control and optical focusing through complex media[1,2]. Coherent light in such media generates randomly scattered light fields that are seen as random three-dimensional (3D) interference patterns, known as speckles[3]. Speckle fields can be manipulated by controlling the incident wavefront to generate enhanced intensity speckles at desired locations. Methods for focusing light through scattering media require an adaptive feedback process or phase conjugation to approximate the optical modes in the random media. Recent methods include wavefront optimization[4–6] and direct inversion of the measured transmission matrix (TM)[7].

Unfortunately, dynamic changes in random scattering media lead to speckle field variations that thwart these processes. The speckle decorrelation time is defined as the time during which the correlation between the speckle field and an initial speckle field remains above a predetermined value. When focusing through scattering media using WFS, the speckle decorrelation reduces the intensity of the obtained focus over time. Dynamic biological tissues are extremely challenging for WFS focusing because fast physical changes such as blood flow reduce decorrelation times to the millisecond range. Typically, WFS is performed using high-resolution liquid crystal (LC) spatial light modulators (SLMs) and deformable mirrors. LC-SLM devices are characterized by refresh rates in the order of 2–100 ms. State-of-the-art methodologies for faster wavefront optimization include micro-electro-mechanical system (MEMS) based mirror arrays[8], the use of binary deformable mirror devices (DMD) in a phase modulation configuration[9,10], optical phase conjugation[11] and a binary ferro-electric LC-SLM[12]. These recent methodologies improve the focusing speed over those of traditional SLM-based techniques but are still limited by the SLM's update rate and the use of a binary phase wavefront that results in a lower enhancement potential. Moreover, phase conjugation focusing suffers from a low signal-to-noise ratio (SNR) compared with feedback-based WFS, because it requires a light source inside or behind the scattering layer[13].

In this Article, we investigate the use of fast 1D SLMs for 2D WFS by taking advantage of the scattering medium to perform a 1D-to-2D transformation. Physically, a highly complex medium randomizes the degrees of freedom by spreading individual 1D modes into uncorrelated 2D speckle fields, and hence provides a means to control the speckle field in space by transforming a 1D optical signal into a 2D signal, as depicted schematically in Fig. 1. Mathematically, the 1D signal utilizes only a fraction of the total degrees of freedom of the incident field[14,15], while scattering, represented by a random TM, spreads these modes irrespective of the particular selection of degrees of freedom. This phenomenon is analogous to the coupling between temporal/spectral and spatial modes in a scatterer[2,15,16].

We utilize a grating light valve (GLV), which is a high-speed 1D MEMs SLM, to speed up feedback-based focusing through complex media. The GLV is composed of thousands of free-standing silicon nitride ribbons on a silicon chip, segmented into 1,088 pixels, each composed of six ribbons as depicted in Fig. 1. By electronically controlling the deflection of the ribbons, the GLV functions as a programmable 1D phase modulator. The GLV allows fast (<300 ns) switching time and high-repetition-rate operation (350 kHz in our case) along with continuous phase modulation. These properties allow three to four orders of magnitude faster operation compared to LC-SLMs, and more than one order of magnitude faster operation compared to binary amplitude DMDs and other binary phase modulators[8–12]. However, utilizing the GLV device for focusing in complex media requires tailored optical design as well as custom software–hardware implementation and signal processing.

This Article is organized as follows: we first describe and analyse the physical principle of 1D-to-2D transformation by a complex medium. We then describe the optical system utilized for WFS focusing in scattering media, and present experiments showing real-time fast focusing in static and dynamic media that is one order of magnitude faster than what was previously possible. We further demonstrate that the technique is appropriate for focusing in multimode fibres (MMFs) and discuss its advantages and limitations.

[1]Department of Electrical, Computer, and Energy Engineering, University of Colorado Boulder, CO, USA. [2]Silicon Light Machines, Sunnyvale, CA, USA.
[3]These authors contributed equally: Omer Tzang, Eyal Niv. *e-mail: omer.tzang@colorado.edu

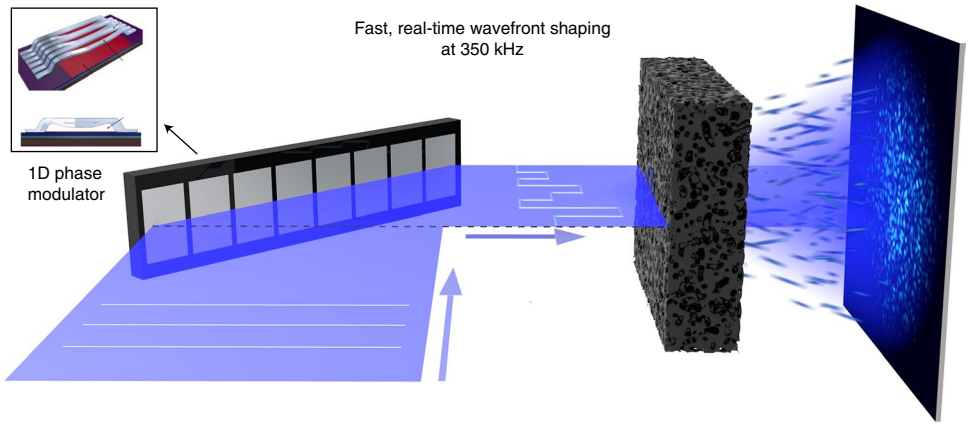

Fig. 1 | Principle of 1D-to-2D transformation for wavefront shaping with a 1D SLM. A collimated and coherent laser beam illuminates the 1D SLM along a line—in our case a 1D MEMS phase modulator operating at 350 kHz, depicted in the top left inset. Using tailored hardware and software implementation, we measure the TM of complex media and focus light through it within 2.4 ms. The system operates continually in real time and allows the examination of rapidly changing media.

1D-to-2D transformation via complex media

Here, we investigate the basis for the use of a 1D phase modulator to enable 2D control of light propagating through complex media. The key observation is that the scattering medium randomly distributes each 1D illuminating mode into a 2D speckle field. Hence, assuming the speckle modes are fully developed, in the sense that the fields are random and uncorrelated, a 1D SLM provides the same 2D degrees of freedom as a 2D SLM with the same number of pixels. Mathematically, on propagation through a thick random scatterer, the 1D and 2D wavefront modulators are essentially equivalent (Supplementary Section 1). Notwithstanding this, it is important to analyse the physical effect of a relatively thin (or relatively weak) scatterer, where the speckle shape is directly affected by the shape of the illumination. We recall that in thin scattering samples, a tilt in the incident beam generates a tilt of the scattered wavefront and the speckle patterns appear correlated within a range of input angles. Similar correlations are also noticed upon spatial shifts or rotation and these phenomena are known as the memory effect[17]. We consider two illumination configurations, as depicted in Fig. 2. The first is the 2D Fourier transform of a square-shaped illumination, in which each pixel of a vertical GLV is imaged and expanded to a horizontal stripe, and is referred to here as Fourier plane illumination. The second configuration is directly the square-shaped illumination, referred to as image plane illumination.

To model the far-field speckle shape generated by a scatterer of variable thickness with modulated 1D illumination, we represent the scattering medium with a TM correlation formulation[18] generalized to 2D fields. The TM model is detailed in the Methods and Supplementary Section 2. In Fig. 2b–d we simulate the Fourier plane illumination. The presence of speckle correlations, or the memory effect, manifests as an elongated speckle grain in the far field, in the orthogonal direction of the illumination line. As the memory effect decreases with a thicker scatterer, the statistics of the speckle field become isotropic. A similar effect and behaviour would be observed with a weak scatterer of given thickness as the scattering mean free path decreases. The corresponding experimental results are presented in Supplementary Section 3. In the case of a thin or weak scatterer, the elongation can be removed by imaging the modulator onto the scatterer with different magnifications along two orthogonal directions, such that the illumination pattern is essentially square-shaped and composed of stripes, as shown in Fig. 2f. This image plane illumination configuration generates round speckles, even with an extremely large memory effect, as shown in Fig. 2g and detailed in Supplementary Section 3.

To quantify the speckle grain elongation, we calculate the autocorrelation of the speckle images and their corresponding average speckle grain size. We define the elongation factor as the ratio of the average grain's major and minor axes. Figure 2i shows that, for the case of Fourier illumination, the elongation factor drops as $1/\sigma$. This is in agreement with the expected elongation in the far field for a corresponding angular spread of σ in the near-field image. Therefore, the Fourier illumination, as defined above, of the scattering sample results in speckle elongation that varies according to the thickness or memory effect of the scattering medium. Interestingly, the anisotropic speckle in thin samples does not reduce the WFS control in the sense that similar enhancement factors are obtained, as shown in Supplementary Section 8.

Experimental set-up

The experimental set-up is depicted in Fig. 3 and described in the Methods. Briefly, the expanded beam generates a line illumination on the GLV after crossing a cylindrical lens. The GLV is placed at an angle, and a collimating cylindrical lens followed by a 4*f* system image the GLV on the back focal plane of a ×10 objective. The scattering sample is located either at the focal plane of the objective, thus being illuminated with the 1D Fourier transform of the expanded GLV phase distribution, or at the image plane by removing the objective lens from the imaging system. We used a source of wavelength 460 nm (532 nm) in the Fourier (image) plane experiments. The speckle field propagates onto a pinhole placed before an avalanche photodiode (APD). The back objective and the pinhole size are selected to match the pinhole to the scattered speckle size. The APD voltage is digitized by a fast data acquisition card (DAQ), then sent to the computer (PC) where it is used to calculate the wavefront using a C++ program that controls all system computation and synchronization. A beamsplitter and camera image the speckle field and focus spot.

For WFS focusing, we select the TM method[9] because it uses a set of predefined phase masks that can be loaded to the GLV memory before operation. Using a preloaded set of phase masks minimizes the data transfer time between the GLV and the PC, allowing the GLV to display all preloaded images at its maximum frame rate. We characterize one column of the TM using three measurements per input mode and calculate one focus spot per cycle. A key element enabling a high-speed system is the elimination of any computational or bandwidth bottlenecks in the feedback loop. We use high-bandwidth data transfer hardware, a dual-port data acquisition scheme and a multi-threaded C++

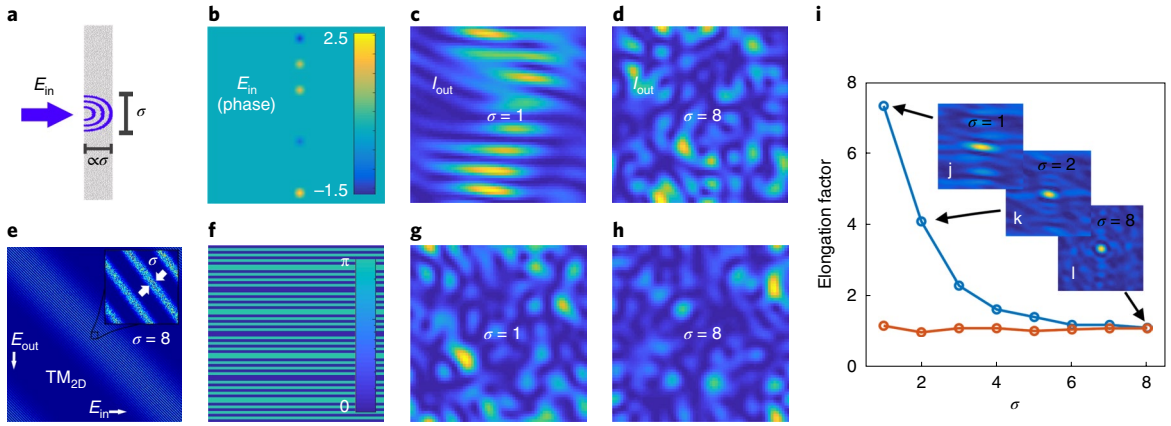

Fig. 2 | Far-field speckle shape for different scatterer widths. a, A beam illuminating a thin slab will cause a diffused spot at the output surface, whose angular spread σ is of the order of the slab thickness. **b**, Fourier plane illumination of the scatterer. A phase map of 1D spots is depicted, representing part of the Fourier transform. The colour bar represents phase values. **c**,**d**, Simulation of speckle fields after propagation of the Fourier plane illumination through a scatterer with $\sigma=1$ and 8, respectively. The images show speckles and represent the calculated intensity of the Fourier transform (far field) of the output near field. **e**, 2D TM corresponding to a scatterer with $\sigma=8$. The image represents the absolute value of the TM and shows a specific band-diagonal structure. **f**, Image plane illumination of the scatterer. The 1D pixels with alternating phases and constant amplitude are expanded to horizontal stripes. The colour bar represents phase values. **g**,**h**, Simulation of speckle fields with image plane illumination for $\sigma=1$ and 8, respectively. **i**, Speckle elongation as a function of the scattering properties of the sample for Fourier plane (blue) and image plane (red) illumination. At each point in the plot, we calculate the speckle elongation as a function of σ, the width of the 2D Gaussian function used to model the TM. This Gaussian function directly relates the scattering sample thickness to the memory effect (angular correlations) and to the far-field shape of the speckles. We plot the elongation factor (ratio of major and minor axes) of the output field autocorrelation, averaged over 100 random realizations. **j**–**l**, Characteristic shapes of speckle autocorrelation with $\sigma=1$, 2 and 8, respectively, for Fourier plane illumination.

application to speed up the focusing process, as described in Supplementary Sections 5 and 6.

The preloaded N input modes, where $N=256$ or 512, are an orthogonal basis of phase patterns displayed on the central part of the GLV. We dedicate groups of GLV pixels for a modulated reference beam, displayed on both outer sides of the GLV, as shown in Fig. 3b. In the experiment, each mode interferes with three phase references (0, π/2 and π), displayed on the frame of the GLV and detected after propagation through the scattering medium by a fast detector. For precise phase measurements, we calibrate the GLV's voltage-to-phase transformation, as described in Supplementary Section 7. After measuring the complex field response for all the input modes, the phase conjugated field is calculated and displayed on the GLV for focusing, similarly to what is done for 2D SLMs[19].

Results

Using a ground glass diffuser with a diffusion angle of ~5° (Thorlabs, DG05-1500) as the scattering medium, we tested the GLV focusing system. Each phase mask was displayed for ~2.8 µs on the GLV, which operated at 350 kHz. Therefore, for $N=256$, all 768 measurements for TM determination occurred in 2.15 ms. The APD signal is digitized and sent to the computer, where the average intensity value for each measurement[20] is used to calculate the TM of the system and display the focusing phase, all within an additional 150 µs. Using the camera image, we calculated the enhancement as the ratio between the peak intensity and the average of the optimized speckle field. Figure 4d illustrates the real-time focusing system using 256 and 512 modes. The focusing sequence takes 2.4 ms and 4.7 ms for the two cases and the focus is kept for another 5 ms before the next measurement sequence. Figure 4b shows an example of a focus spot with 256 modes, demonstrating enhancement of 44× over the background level. Figure 4c shows the results obtained with 512 modes and a signal enhancement of 72×. Figure 4e shows a statistical analysis of the enhancement as a function of the number of modes, as described in the Methods and Supplementary Section 4. Supplementary Video 1 shows continuous

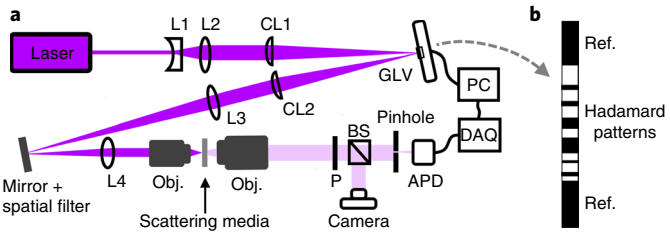

Fig. 3 | Experimental set-up. a, A laser beam illuminates the GLV. The imaging system of the GLV comprises a conjugate lens pair with an aperture in the Fourier plane between the lenses. The GLV image is created at the back aperture of the ×10 objective and focused onto the scattering sample. A ×20 objective images a plane behind the scattering sample. This image propagates to a pinhole placed before an APD. The APD signal is sent to a fast DAQ before being processed by a PC to create a focusing wavefront. A camera and beamsplitter (BS) capture the focal spot image. L1–L4 are lenses with corresponding focal lengths of −50 mm, 300 mm, 300 mm and 50 mm; CL1–2 are cylindrical lenses with focal lengths of 150 mm. Obj., objectives; P, polarizer. The set-up is used for Fourier plane illumination and can be configured for image plane illumination by removing the objective lens before the scattering medium. **b**, An example of a phase distribution for a single 1D Hadamard basis element, surrounded by a phase reference for TM measurement.

focusing while the scatterer is shifted laterally. To test our system on controlled dynamic samples, we prepared scattering solutions with controlled viscosity—and therefore varying speckle decorrelation times that mimic dynamic biological tissues, as described in the Methods. Figure 4f and Supplementary Video 2 show continuous focusing through dynamic samples. We also tested the system with chicken breast and titanium oxide nanoparticles, as described in Supplementary Section 4.

Finally, we tested our system for focusing coherent light at the output of a MMF, a similar scenario to speckle focusing in random

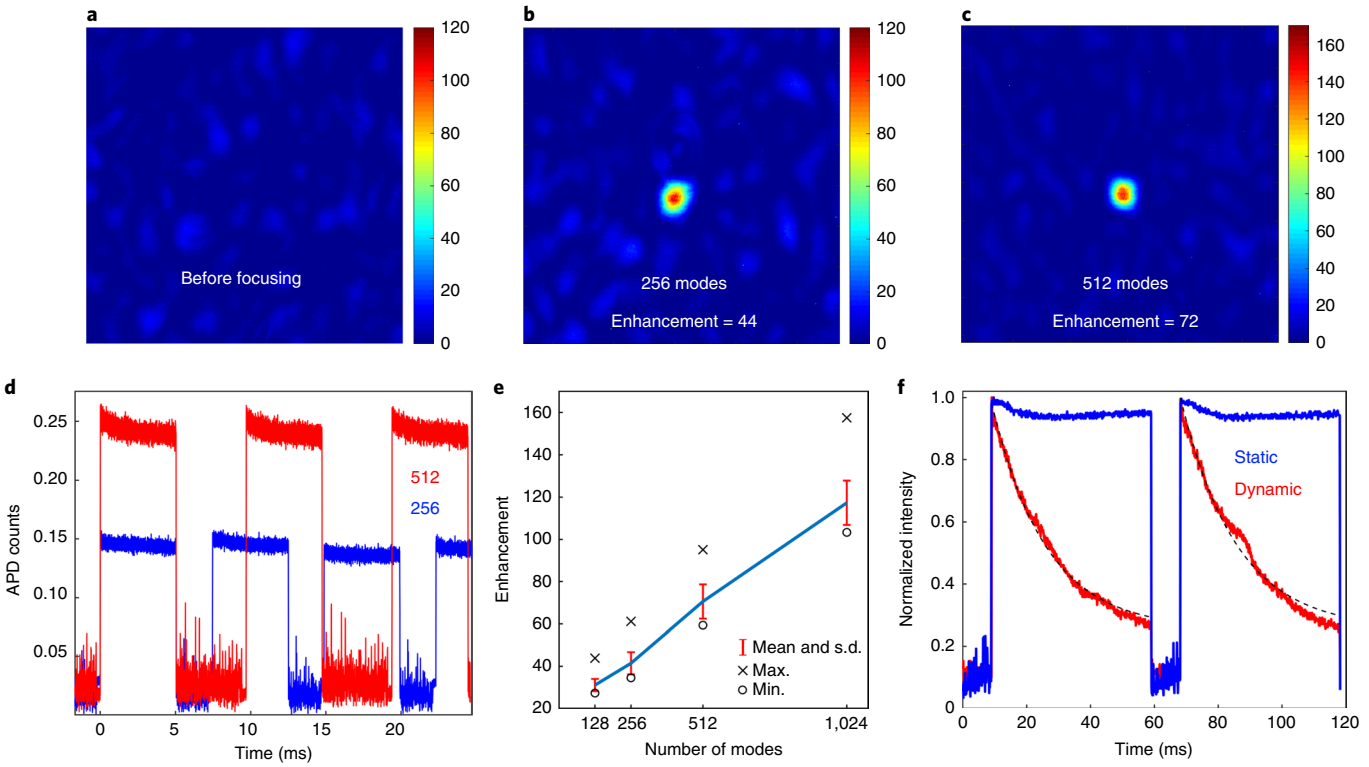

Fig. 4 | System performance in terms of focus enhancement versus time. a, Speckle image before wavefront optimization. **b**, Focal spot snapshot after wavefront optimization with 256 modes and image plane illumination. The wavefront was displayed continually, and the reference beam was blocked by placing a high-spatial-frequency grating on the reference pixels and blocking diffraction of the beam at the Fourier plane using a slit. **c**, Focal spot with 512 modes. Colour bars represent the intensity on the camera. **d**, Real-time focusing through a static diffuser using 256 modes (blue) and 512 modes (red). **e**, Enhancement versus number of modes using a static diffuser. The error bars show s.d. and the circles and crosses show the minimal and maximal values (see Methods for details). **f**, Continuous focusing through dynamic samples with different decorrelation times using 1,024 modes. The blue curve shows a static sample with gelatin and lipid concentrations of 2.5 mg ml^{-1} and 0.5%. The red curve shows a diluted solution with gelatin and lipid concentrations of 5 μg ml^{-1} and 0.01%. A decorrelation time of ~17 ms was measured using an exponential curve fit (black). Wavelength, 532 nm.

scattering media. In MMFs, the propagation of light is described by superpositions of propagating modes. Phase-velocity mode dispersion and random mode coupling arising from imperfections and bends contribute to creating complex 3D interference patterns observed as speckles at the fibre output. In the set-up, we replace the scattering medium with a 30 cm multimode fibre, including input and output coupling optics. The algorithm and system used for MMF optimization were similar. For optimal results, we adjusted the coupling optics and imaged the GLV into the fibre with a size-matched magnification that coupled well all the GLV pixels. Figure 5 shows far-field images of the fibre output before and after GLV optimization where a selected speckle is enhanced. The speckle field at the output of the MMF contains well-developed round speckles even with Fourier plane illumination due to the low memory effect of the long fibre. The real-time, high-speed control is critical for maintaining a focus at the output of a rapidly moving fibre[10], for in vivo imaging[21] or for controlling nonlinearities in MMFs[22].

For WFS focusing, we initially selected the TM method, because it uses a set of predefined phase masks that can be loaded to the GLV memory before operation and uses only three phase measurements for each mode. The focusing phase mask in TM is a calculated phase conjugated wavefront. The accuracy of this calculation may be reduced due to the non-ideal structure of the GLV, leading to lower enhancement. Therefore, we tested a second iterative algorithm that does not rely on a direct phase conjugation calculation. Our iterative algorithm, implemented at a full GLV speed of 350 kHz, finds the phase of each Hadamard mode directly by measuring a set of 16 phase-shifted patterns for each mode, and selecting the one with maximal enhancement. Because the Hadamard patterns are orthogonal, summing all the optimized modes generates a bright focus through the scattering medium at the desired location.

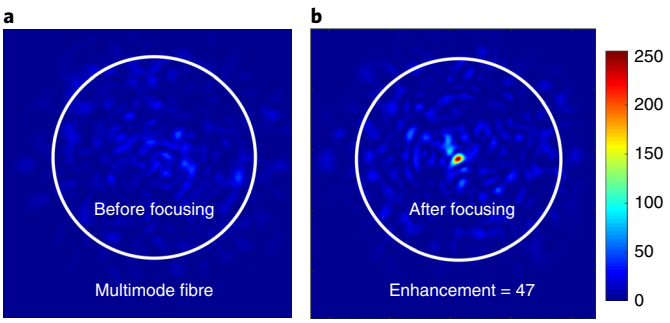

Fig. 5 | Focusing at the output of a MMF. a, Far-field image of the fibre output before wavefront optimization. **b**, Image after wavefront optimization. The images were recorded at full GLV speed using 256 modes. Colour bar represents the intensity on the camera. The fibre is a graded-index MMF with a diameter of 50 μm, ~800 modes, length of 30 cm and wavelength of 532 nm. We used Fourier plane illumination and the enhancements are comparable to the case of other scattering media. The white circle indicates the fibre core.

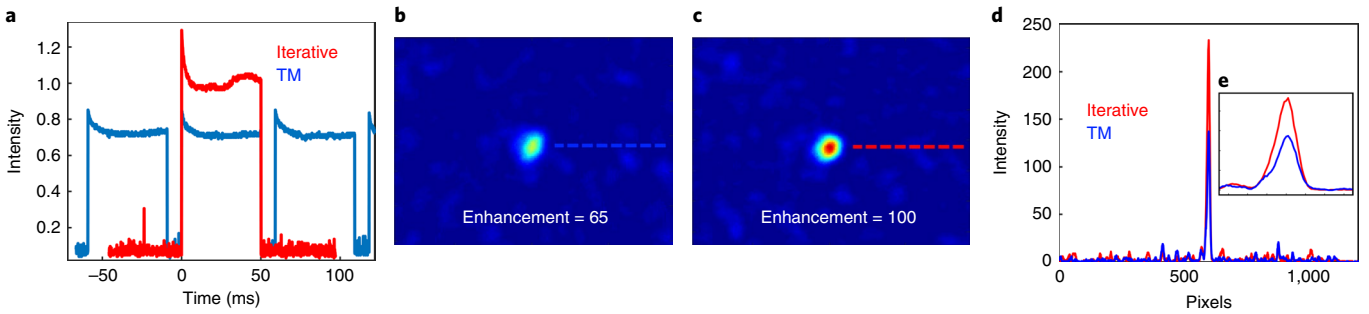

Fig. 6 | Comparison of the iterative algorithm and the TM method. a, Real-time focusing using the TM method with 1,024 modes (blue) and a single cycle of the iterative algorithm using 16 phase steps for each of the 1,024 Hadamard modes (red). Note that the calculation time increases by ~5 times in the iterative algorithm. **b**, Focal spot snapshot after wavefront optimization with TM. **c**, Focal spot snapshot after wavefront optimization with iterative focusing. We kept the camera parameters constant in both snapshots for comparison. The scattering medium is a thin diffuser, placed in the image plane of the GLV and illuminated with a square GLV image to generate round speckles. **d**, Focal spot cross-sections. The blue and red plots correspond to the cross-sections indicated by the dotted blue and red lines in **b** and **c**, respectively. **e**, Enlarged view of the cross-section in **d**. The experiments were performed with a 532 nm laser.

We selected this particular algorithm over other known alternatives only because it uses a preloaded set of phase masks, allowing the GLV, with our current hardware, to display all preloaded images at its maximum frame rate. The results, depicted in Fig. 6, show that the iterative algorithm improves the enhancement by ~50% compared to the TM algorithm. However, because the number of measurements increases, the time duration also increases by 16/3, namely by the ratio of the phase measurements. However, the enhancement improvement is encouraging as it shows that with improved modelling of the non-ideal characteristics of the GLV, or better algorithms, implemented in the GLV hardware, the system can achieve better performance.

Discussion

The results presented herein show a system design enabling the use of high-speed 1D SLMs for WFS. The concept of a 1D-to-2D scattering transformation provides a framework for understanding and designing these WFS systems. Further system performance improvements are possible by taking into account the non-ideal characteristics of the GLV. In what follows, we discuss some of these areas that are open for improvement.

The complex amplitude of the field at the desired focus area may be regarded as resulting from the sum of contributions from many elementary scattering areas[3] $A(x,y,x)=\sum_{k=1}^{N}|a_k|exp(i\phi_k)$. In our system, each of the k independent speckle fields is produced by an orthogonal mode, displayed on the GLV. For N modes, the phasor amplitude of the optimized field—with all ϕ_k phases perfectly aligned—can theoretically reach an enhancement proportional to N. If there is not full control of the phase over 2π rad or there is a high noise level[23], the enhancement is lower and might not scale with N.

Still, we observed that the enhancement is lower than that obtained using a phase-only LC-SLM or DMD for the same number of pixels[24], and ~20% of the ideal value of a perfect modulation in the absence of noise. Apart from sources of noise in the measurement[25], mechanical instabilities and common non-ideal aspects of SLMs such as distortion of the wavefront due to the pixel array structure, the existence of unmodulated light and other wavefront distortions[6], the GLV incorporates a combination of additional features that require careful modelling when operated as a phase modulator. We analyse these features in detail in Supplementary Section 8 and determine via simulations and characterization experiments that the most significant one is the low fill factor due to inter-pixel gaps that generates a residual modulated background signal.

Each GLV pixel contains six ribbons that move up and down together, as described in Supplementary Sections 6 and 8. The spacing between ribbons creates reflections from the back surface that interfere coherently and generate an additional higher-frequency grating. The efficiency of this residual diffraction grating changes with the ribbons' displacement and reaches 5–10% of a GLV pixel grating diffraction. Consequently, we observe that increasing the ratio of signal pixels that are static in the experiment versus reference pixels improves the focusing enhancement. For example, signal to reference pixel ratios of 70% and 95%, for the 256 and 512 modes, respectively, increased the overall SNR of mode interference, improved the accuracy of the measurement and generated better enhancements. In addition, to improve the GLV performance, the back surface could be coated to minimize unwanted reflections.

In the TM optimization, we used either Hadamard or Fourier basis sets, with both showing similar performance. The illumination optics in our set-up includes two cylindrical lenses that may cause astigmatism if their orientation is even slightly mismatched and may contribute to speckle elongation in thin samples. Additionally, the inhomogeneous Gaussian illumination of the 1D SLM using cylindrical lenses, even when the beam is expanded beyond the GLV, distributed a non-uniform intensity across the GLV pixels. When the TM modes are summed linearly in the focusing calculation, a phase error reduces the enhancement. This issue could be addressed by flat illumination using a Powell lens or corrected computationally.

It is important to comment that the speed of focusing in scattering media is limited not only by the speed of the modulator and calculations, but also by the photon budget and SNR. We used a high-transmission scattering layer and had sufficient, but not optimal, detector SNR for fast optimization of a single speckle. In other low-SNR scenarios, such as weak fluorescence deep inside tissue, signal averaging could limit the overall speed.

Interestingly, the 1D-to-2D transformation we investigated can be generalized to higher dimensionality because the random media distribute the available degrees of freedom to 3D space and 4D space–time. Therefore, a 1D modulator can be used to control spatiotemporal[2,15,16] and spectral[22] properties of light in complex media.

Conclusions

We have demonstrated high-speed wavefront optimization for focusing through complex media using a fast 1D SLM with fast data acquisition and software adapted to the task. With this approach, we have demonstrated an order of magnitude improvement in measurement speed over the current fastest feedback wavefront determination method and four orders of magnitude improvement over

LC-SLM methods[2]. We have also demonstrated real-time focusing through turbid materials during scanning, focusing through dynamic scattering media and control of light at the output of MMFs, which is of major interest in minimally invasive endoscopy. The improved speed is a significant technological step forward and holds potential for wide-field, video-rate focusing and imaging in dynamic scattering media as well as high-speed control in MMFs. The concept of 1D-to-2D scattering transformation provides insight into the speckle correlations and shape in WFS while guiding the design and utilization of WFS systems.

Online content

Any methods, additional references, Nature Research reporting summaries, source data, statements of code and data availability and associated accession codes are available at https://doi.org/10.1038/s41566-019-0503-6.

Received: 27 August 2018; Accepted: 4 July 2019;
Published online: 26 August 2019

References

1. Vellekoop, I. M. & Mosk, A. P. Focusing coherent light through opaque strongly scattering media.*Opt. Lett.* **32**, 2309–2311 (2007).
2. Mosk, A. P., Lagendijk, A., Lerosey, G. & Fink, M. Controlling waves in space and time for imaging and focusing in complex media. *Nat. Photon.* **6**, 283–292 (2012).
3. Goodman, J. W. Some fundamental properties of speckle. *J. Opt. Soc. Am.* **66**, 1145–1150 (1976).
4. Vellekoop, I. M., Lagendijk, A. & Mosk, A. P. Exploiting disorder for perfect focusing. *Nat. Photon.* **4**, 320–322 (2010).
5. Katz, O., Small, E. & Silberberg, Y. Looking around corners and through thin turbid layers in real time with scattered incoherent light. *Nat. Photon.* **6**, 549–553 (2012).
6. Vellekoop, I. M. Feedback-based wavefront shaping. *Opt. Express* **23**, 12189 (2015).
7. Popoff, S., Lerosey, G., Fink, M., Boccara, A. C. & Gigan, S. Image transmission through an opaque material. *Nat. Commun.* **1**, 81 (2010).
8. Blochet, B., Bourdieu, L. & Gigan, S. Focusing light through dynamical samples using fast continuous wavefront optimization. *Opt. Lett.* **42**, 4994–4997 (2017).
9. Conkey, D. B., Caravaca-Aguirre, A. M. & Piestun, R. High-speed scattering medium characterization with application to focusing light through turbid media. *Opt. Express* **20**, 1733–1740 (2012).
10. Caravaca-Aguirre, A. M., Niv, E., Conkey, D. B. & Piestun, R. Real-time resilient focusing through a bending multimode fiber. *Opt. Express* **21**, 12881–12887 (2013).
11. Wang, D. et al. Focusing through dynamic tissue with millisecond digital optical phase conjugation. *Optica* **2**, 728–735 (2015).
12. Liu, Y., Ma, C., Shen, Y., Shi, J. & Wang, L. V. Focusing light inside dynamic scattering media with millisecond digital optical phase conjugation. *Optica* **4**, 280–288 (2017).
13. Popoff, S. M., Lerosey, G., Fink, M., Boccara, A. C. & Gigan, S. Controlling light through optical disordered media: transmission matrix approach. *New J. Phys.* **13**, 123021 (2011).
14. Piestun, R. & Miller, D. A. B. Electromagnetic degrees of freedom of an optical system. *J. Opt. Soc. Am. A* **17**, 892–902 (2000).
15. Mccabe, D. J. et al. Spatio-temporal focusing of an ultrafast pulse through a multiply scattering medium. *Nat. Commun.* **2**, 447 (2011).
16. Katz, O., Small, E., Bromberg, Y. & Silberberg, Y. Focusing and compression of ultrashort pulses through scattering media. *Nat. Photon.* **5**, 372–377 (2011).
17. Freund, I., Rosenbluh, M. & Feng, S. Memory effects in propagation of optical waves through disordered media. *Phys. Rev. Lett.* **61**, 2328–2331 (1988).
18. Judkewitz, B., Horstmeyer, R., Vellekoop, I. M., Papadopoulos, I. N. & Yang, C. Translation correlations in anisotropically scattering media. *Nat. Phys.* **11**, 684–689 (2015).
19. Popoff, S. M. et al. Measuring the transmission matrix in optics: an approach to the study and control of light propagation in disordered media. *Phys. Rev. Lett.* **104**, 100601 (2010).
20. Freischlad, K. & Koliopoulos, C. L. Fourier description of digital phase-measuring interferometry. *J. Opt. Soc. Am. A* **7**, 542–551 (1990).
21. Ohayon, S., Aguirre, A. M. C., Piestun, R. & DiCarlo, J. J. Minimally invasive multimode optical fiber microendoscope for deep brain fluorescence imaging. *Biomed. Opt. Express* **9**, 1492–1509 (2018).
22. Tzang, O., Caravaca-Aguirre, A. M., Wagner, K. & Piestun, R. Adaptive wavefront shaping for controlling nonlinear multimode interactions in optical fibres. *Nat. Photon.* **12**, 368–374 (2018).
23. Akbulut, D., Huisman, T. J., Putten, E. G. Van., Vos, W. L. & Mosk, A. P. Focusing light through random photonic media by binary amplitude modulation.*Opt.Express* **19**, 4017–4029 (2011).
24. Conkey, D. B., Brown, A. N., Caravaca-Aguirre, A. M. & Piestun, R. Genetic algorithm optimization for focusing through turbid media in noisy environments.*Opt. Express* **20**, 4840–4849 (2012).
25. Yılmaz, H., Vos, W. L. & Mosk, A. P. Optimal control of light propagation through multiple-scattering media in the presence of noise. *Biomed. Opt. Express* **4**, 1759–1768 (2013).

Acknowledgements

We thank L. Eng, A. Payne and Y. Hashimoto from Silicon Light Machines as well as S. Gigan for useful discussions. This work was supported by NSF awards nos. 1548924 and 1611513 and NIH grant no. REY026436A.

Author contributions

R.P. conceived the project. O.T. and E.N. initiated and designed the project. O.T. and S.S. built the set-up. E.N. designed the software. G.M. designed the GLV hardware modifications. O.T. and S.S. performed the experimental work. S.L., S.S. and O.T. performed the simulations. O.T., S.L., S.S. and R.P. discussed the experiments and data. O.T. wrote the manuscript with contributions from all authors. O.T. and R.P. supervised the project.

Additional information

Supplementary information is available for this paper at https://doi.org/10.1038/s41566-019-0503-6.

Reprints and permissions information is available at www.nature.com/reprints.

Correspondence and requests for materials should be addressed to O.T.

Publisher's note: Springer Nature remains neutral with regard to jurisdictional claims in published maps and institutional affiliations.

Methods

Experimental set-up. For illumination, we used a 20 mW, 460 nm continuous-wave (c.w.) laser (New Focus, Vortex plus TLB 6800) for Fourier plane illumination, and a 532 nm c.w. laser (Coherent, Verdi G5) for image plane illumination. The expanded beam generated a line illumination on the GLV (x direction) after crossing a cylindrical lens. The GLV (F1088-P-HS) is placed at a reflection angle of ~10°. A collimating cylindrical lens and a ×6 demagnifying 4f system were used to image the GLV (expanded in the y direction) on the back focal plane of a ×10 objective. We tested two illumination configurations. First, the scattering sample was located at the focal plane of the objective, and was thus illuminated with the 1D Fourier transform of the GLV phase distribution. Second, a configuration of GLV image plane illumination was used in which the second lens of the 4f system imaged the GLV on the scattering sample.

A ×20 (NA = 0.4) objective was used to image a plane behind the scattering sample. The speckle field propagated onto a pinhole placed before an APD. The back objective and the pinhole size were selected to match the pinhole to the scattered speckle size. The APD voltage was digitized by a fast DAQ (Alazartech, ATS9350) and sent to the PC where it was used to calculate the wavefront with a C++ program that controlled all system computation and synchronization. A non-polarizing BS reflected 1% of the light onto a camera (Point grey, Chameleon) to image the speckle field and focus spot. In the experiment shown in Fig. 5, we used a graded-index MMF (Newport F-MSD).

TM model. The TM model for 1D illumination of scattering samples with the memory effect took into account random scattering by modelling an uncorrelated random matrix between the 2D input and output fields, S_{2D}. The memory effect was modelled by multiplying (point by point) S_{2D} by a band-diagonal matrix G_{2D} that established different degrees of the memory effect (Supplementary Section 2). To generate G_{2D} we used a Gaussian filter whose width σ was proportional to the degree of memory effect and, in turn, the scatterer thickness[18]. The full TM model is detailed in Supplementary Section 2 and an example of the TM is depicted in Fig. 2e.

Statistical analysis of the enhancement. To analyse the enhancement, we recorded videos of continuous focusing through a diffuser while translating the position of the output speckle with respect to the APD using a mirror. In each video, we changed the number of modes used for TM focusing. In the data processing, we automatically selected 500 frames out of ~2,000 frames in each video based on the following criteria. First, we removed frames in which the focus was located at the edge of the speckle field because the negligible background beyond the speckle field led to amplified enhancement. These frames were removed by thresholding the deviation of the mean pixel value in all the frames. Second, we removed low-enhancement frames in which the pre-optimization reference speckle was weak. As can be observed in Supplementary Video 1, weak pre-optimization reference speckles typically lead to smaller enhancements and should be avoided. Effectively, the statistical analysis represents 500 focusing optimizations of speckle grains with a measurable reference signal.

Preparation of dynamic samples. The dynamic samples were composed of gelatin, water and intra-lipid. By varying the concentration of gelatin and intra-lipid, we controlled the viscosity and thus the dynamic scattering properties of our samples. Sample preparation included heating 10 ml of water to 40 °C and dissolving 50 mg of gelatin (ACROS gelatin type A) and 0.5 ml of intralipid (20% solution) to form a uniform solution. The prepared samples were cooled, diluted further and mounted in a depression concave slide or a glass cuvette to form a volume scattering sample with controlled decorrelation times.

Data availability

The data that support the plots within this paper and other findings of this study are available from the corresponding author upon reasonable request.